



Published by Fusion Energy Division, Oak Ridge National Laboratory
Building 5700 P.O. Box 2008 Oak Ridge, TN 37831-6169, USA

Editor: James A. Rome
E-Mail: jar@ornl.gov

Issue 106
Phone (865) 482-5643

November 2006

On the Web at <http://www.ornl.gov/sci/fed/stelnews>

A study of pulse propagation in a simplified critical gradient model

Over the last few years, we have been developing an alternative model for the description of transport in fusion plasmas. It is generally believed that stiff models can be used to explain many of the unusual transport effects reported over the last two decades qualitatively, in both tokamaks and stellarators. Therefore, stiffness (introduced via a critical gradient mechanism) may be an essential ingredient for any useful transport model, and may help in understanding non-standard transient transport behavior.

Furthermore, the standard simplified transport description in terms of diffusion and convection appears unsatisfactory in the sense that differing experimental configurations (e.g., on/off-axis heating, different machine sizes) seem to require different transport parameter choices, which is indicative of the fact that the simplified description may not capture all the essential physics. Therefore, including stiffness may also be important for correct extrapolations of global transport properties to larger devices.

The starting point for this work has been the Continuous-Time Random Walk, which provides a description of diffusive transport processes at a very fundamental level, and which leads to the Generalized Master Equation. Notably, this approach avoids making assumptions about locality of the transport processes and allows critical gradient mechanisms to be treated in a mathematically sound manner. It is generally accepted that critical gradient mechanisms are fundamental for understanding transport in fusion plasmas [1–3].

The Generalized Master Equation is, in simplified form for one dimension (x) and one transported field [the particle density $n(x,t)$] [1]:

$$\frac{\partial}{\partial t}n(x,t) = \frac{1}{\tau_D} \int_0^1 p(x-x';x',t)n(x',t)dx' - \frac{n(x,t)}{\tau_D} + S(x,t) \quad (1)$$

where τ_D is a “waiting time” (average time before a particle takes a step), $p(x-x';x',t)$ the probability of the particle moving from x' to x at time t , and $S(x,t)$ a particle source. This equation reduces to the usual diffusion equation in the appropriate (local) limit [4]. The critical gradient mechanism is introduced by letting the step distribution p depend on the local gradient:

$$p = p_0 + \Theta[|\nabla n| - \kappa](p_1 - p_0),$$

In this issue . . .

A study of pulse propagation in a simplified critical gradient model

Stiffness (a critical gradient) may be an essential ingredient for any useful (simplified) transport model and may help to explain both non-standard transient and global transport behavior; understanding stiffness may be fundamental for proper transport extrapolations to larger devices. We explore the propagation of perturbations in a simplified but stiff transport model controlled by a critical gradient, producing effects very similar to those observed in real-life experiments (recently also in stellarators). 1

Five years of WEGA operation at IPP Greifswald

The Wendelstein Experiment in Greifswald für die Ausbildung (education) is a medium-sized classical stellarator operated at the Max-Planck-Institut für Plasmaphysik, Greifswald branch. This year, the fifth anniversary of first plasma operation of WEGA (on 20 July, 2006) and the attainment of 20,000 shots (on 10 November, 2006) were celebrated. On this occasion we give an overview of selected results. 4

Stellarator Workshop database

CIEMAT is publishing a database of the proceedings of past Stellarator Workshops 10

All opinions expressed herein are those of the authors and should not be reproduced, quoted in publications, or used as a reference without the author's consent.

Oak Ridge National Laboratory is managed by UT-Battelle, LLC, for the U.S. Department of Energy.

where $p_0(x - x')$ is a step distribution (taken independent of the location x' and time t for simplicity) generating the subcritical transport, $p_1(x - x')$ a step distribution for supercritical transport, $\Theta[z]$ is the Heaviside function, and κ is the critical gradient.

Previous work has shown that this model produces (a) stiff profiles (profile consistency), (b) power degradation, (c) rapid transport phenomena, (d) changing system size scaling (reminiscent of the Bohm/gyro-Bohm scaling transition) [1], and (e) “uphill” transport [5], all of which are phenomena generally observed in thermonuclear fusion experiments. It was found that the main cause for the uphill transport phenomenon is the critical mechanism itself, and that the precise choice of transport mechanism (or type of step distribution) for the supercritical and subcritical transport channels is of minor importance, at least for this particular phenomenon [6]. It was also established that describing the global behavior of a system with a critical gradient (i.e., the steady-state profiles) requires dynamical simulations; predicting the steady-state profiles without doing so turns out to be difficult, if not impossible [7]. Progress in the understanding of transport in the presence of a critical gradient therefore requires the development of transport models that may be simplified in many respects, but noting that the critical mechanism cannot be replaced by any simple time-average “equivalent” description. The model developed so far falls precisely in this category.

In the present work, we continue to strive for further understanding of critical gradient models by studying the propagation of perturbations [8]. An example of the propagation of perturbations is shown in Fig. 1. Shown are color plots of the density perturbation vs time and space for a sequence of cases with increasing fuelling rate $S(x,t) = S_0$. The system is symmetric with respect to $x = 1/2$ (the “axis”). At a low fuelling rate, the system is subcritical, and transport is diffusive. As the fueling rate is increased, an ever-larger fraction of the system becomes critical. The critical region grows from the edge inward. The system is allowed to relax to steady state before a negative perturbation is created (left-right symmetric). The plots show the time evolution of the perturbation. In the first three cases, with low fueling rates ($S_0 = 0.01, 0.02, 0.05$), the perturbation spreads and its amplitude decays (not visible on the short time scale shown here). Interestingly, outside the zone of the negative perturbation, a positive pulse develops that propagates in advance of the negative perturbation. This pulse is generated by flux accumulation in the region between supercritical (fast) and subcritical (slow) transport zones. The positive pulse first propagates ballistically, and then slows down (when the local gradients have decayed sufficiently), to continue spreading diffusively.

With stronger fueling ($S_0 = 0.1$), the starting point of the positive pulse is decoupled from the negative pulse. This is caused by the fact that the profile is now critical in the range $0.7 < x \leq 1$ (and symmetrically in the left system

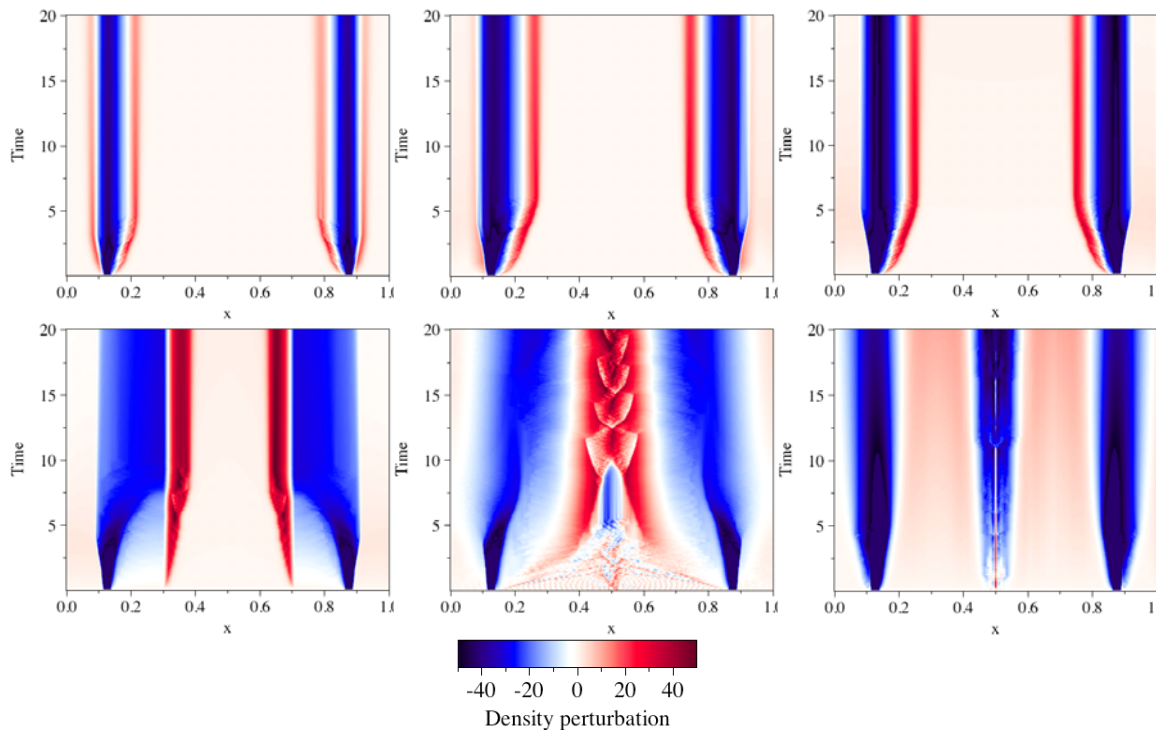


Fig. 1. Evolution of perturbation (introduced at $t = 0$) in space and time, for cases (left to right, top to bottom): $S_0 = 0.01, 0.02, 0.05; 0.1, 0.2, 0.5$; p_0 and p_1 Gaussian.

half). Because of the Heaviside function in Eq. (1), the profile is extremely stiff in this region, causing nearly instantaneous propagation and producing this pulse decoupling effect. At even larger values of the fuelling rate, the critical region covers virtually the whole system, and very complex behavior is observed. We note that the nearly immediate central response to an edge perturbation and the sign reversal of the pulse amplitude have both been observed in actual experiments (recently also in stellarators, see Ref. [9]). An attempt at modeling this complex behavior using a single fractional differential equation with fixed coefficients did not succeed [8], confirming the previous statement that the critical gradient mechanism should not be treated in an oversimplified manner, but needs to be handled by performing dynamical simulations.

These observations are believed to be relevant for understanding transport in fusion devices, where critical mechanisms are thought to be operative, and profile stiffness and the concomitant power degradation are often observed.

Extension of the single-field model to two fields (density and temperature), as proposed in Ref. [10] is in progress.

B. Ph. van Milligen
Asociación EURATOM-CIEMAT para Fusión
Avda. Complutense 22, 28040 Madrid, Spain
E-mail: boudewijn.vanmilligen@ciemat.es

R. Sánchez, B. A. Carreras
Fusion Energy Division, Oak Ridge National Laboratory
P.O. Box 2001, Oak Ridge TN 37831-2001, USA
E-mail: sanchezferlr@ornl.gov, carrerasba@ornl.gov

References

- [1] B. van Milligen, R. Sánchez, and B. Carreras, *Phys. Plasmas* **11**, 2272 (2004).
- [2] D. Baker, C. Greenfield, K. Burrell, J. DeBoo, E. Doyle, R. Groebner, T. Luce, C. Petty, B. Stallard, D. Thomas, and Mr. R. Wade, *Phys. Plasmas* **8**, 4128 (2001).
- [3] G. Hoang, C. Bourdelle, X. Garbet, G. Giruzzi, T. Aniel, M. Ottaviani, W. Horton, P. Zhu, and R. Budny, *Phys. Rev. Lett.* **87**, 125001 (2001).
- [4] R. Sánchez, B. van Milligen, and B. A. Carreras, *Phys. Plasmas* **12**, 056105 (2005).
- [5] B. van Milligen, B. A. Carreras, and R. Sánchez, *Phys. Plasmas* **11**, 3787 (2004).
- [6] J. Gavnholt, J. Rasmussen, O. Garcia, V. Naulin, and A.H. Nielsen, *Phys. Plasmas* **12**, 084501 (2005).
- [7] L. Krupnik, et al., "The Heavy Ion Beam Probing Development for WEGA Stellarator," *Fusion Science and Technology*, **50** (2006) 276–280.
- [8] B. van Milligen, B. A. Carreras, V. E. Lynch, and R. Sánchez, *Proc. 21st IAEA Fusion Energy Conf., TH/P2-17* (2006).
- [9] N. Tamura, S. Inagaki, T. Tokuzawa, K. Tanaka, C. Michael, T. Shimozuma, S. Kubo, K. Ida, K. Itoh, D. Kalinina, et al., *Proc. 21st IAEA Fusion Energy Conf., EX/5-6* (2006).
- [10] B. van Milligen, B. A. Carreras, and R. Sánchez, *Plasma Phys. Control. Fusion* **47**, B743 (2005).

Five years of WEGA operation at IPP Greifswald

The Wendelstein Experiment in Greifswald für die Ausbildung (education), or WEGA, is a medium-sized classical stellarator operated at the Max-Planck-Institut für Plasmaphysik Greifswald branch. This year, the 5th anniversary of first plasma operation of WEGA (on 20 July, 2006) and the attainment of 20,000 shots (on 10 November 2006) were celebrated. On this occasion we give an overview of selected results.

Overview

The WEGA is probably one of the longest used experiments in fusion research. Originally WEGA was designed as a hybrid experiment for studies of lower hybrid heating scenarios in both a tokamak and a stellarator configuration within the framework of collaboration between France and Germany. In 1975 the machine entered service in Grenoble, France, in the tokamak configuration and was used almost exclusively in this configuration until the end of operation there. Later in the 1980s the machine was operated at the Institut für Physik at the University of Stuttgart as a stellarator. In 2000 the machine came to the Greifswald branch of the Max-Planck-Institut für Plasmaphysik and was rebuilt under the leadership of Johann Lingertat in the stellarator configuration. The first stellarator plasma was generated on 13 July 2001. The main objectives of the experiment, which is integrated in the division of Friedrich Wagner, are the training of students, the testing of diagnostics and infrastructure for Wendelstein 7-X (W7-X), and for basic plasma research. Furthermore, the control system of W7-X will be tested on WEGA.

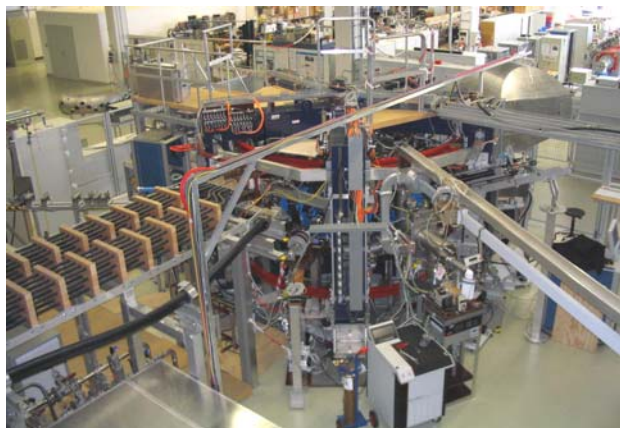


Fig. 1. The WEGA stellarator, located at the Max-Planck-Institut für Plasmaphysik, Greifswald branch, Germany.

The plasma vessel of the WEGA stellarator has a major radius $R = 72$ cm and a minor radius $r = 19$ cm. The maxi-

imum effective plasma radius r_{eff} is about 11 cm. The magnetic field coil system consists of 40 toroidal field coils, 4 helical field coils, and 2 pairs of vertical field coils. The helices have $l = 2$ poloidal period and $m = 5$ toroidal period. Furthermore, the machine is equipped with a 5-period ohmic transformer, but this is not currently in use. The machine can be operated steady state up to a field strength of $B = 0.4$ T at low iota pulses. Maximum field strength of 0.9 T can be achieved in pulsed operation.

The following diagnostics are operational: a residual gas analyzer, Langmuir probes (single and array) on slow or fast manipulator, high-frequency probes, H_{α} detector, single-channel interferometer, coherent imaging spectrometer (CIS), optical overview spectrometer, bolometer [1], Soft X-ray detector, and video diagnostics. Further diagnostics in preparation include a neutral gas manometer, a diamagnetic loop, a laser-induced fluorescence system, and a heavy ion beam probe (HIBP). Many of the diagnostics are being tested for use on W7-X.

Flux Surface Measurements

In the first campaign the vacuum magnetic flux surfaces were determined with the fluorescent technique using a small electron gun emitting electrons parallel to the magnetic field vector. For the mapping of electron beam with energy of up to 300 V, a wire ellipse coated with fluorescent ZnO powder could be moved over the whole vessel cross section, resulting in a Poincaré plot. The experiments were carried out scanning a wide range of rotational transform, $0.1 \leq \iota \leq 1$, by changing the current in the helical field coils at a constant toroidal field $B = 87.5$ mT. It was found that closed and nested magnetic flux surfaces of good quality exist up to $\iota = 1$. However, field errors, probably due to a misalignment between the helical and the toroidal field coils, give rise to magnetic islands with mode numbers $m = 1$ and $m = 2$. An example is shown in Fig. 2; the magnetic flux surfaces for $\iota_0 = 1/3$ are disturbed by non-natural islands caused by these unwanted error fields [2]. The size and phase of the magnetic islands can be varied using an additional planar field coil [3].

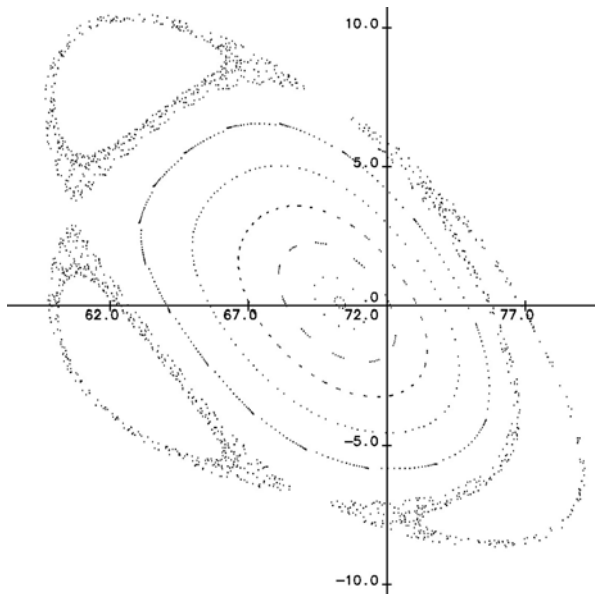
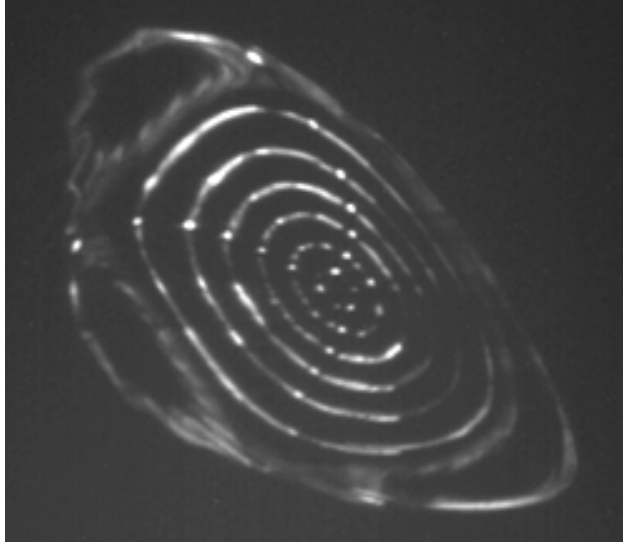


Fig. 2. Measured (top) and computed (bottom) magnetic surfaces for $\tau_0 = 1/3$.

The experimental results are in good agreement with results from calculations using the Gourdon and the W7 field line tracing codes [4, 5].

In preparation for the magnetic flux surface diagnostic on W7-X, a modified electron beam technique that makes magnetic field lines visible was tested. The method is based on the collisional interaction of an electron beam with a highly diluted gas and results in the emission of visible light along the trajectory of a magnetic field line. Optimum conditions for the visible length of the light trace were obtained in argon and hydrogen at a pressure of $p = 1.5 \times 10^{-4}$ mbar, the highest possible accelerating voltage of 450 V, and a maximum magnetic field strength of B

$= 0.5$ T. Up to 15 toroidal turns of the field line in parallel and antiparallel directions equal to a length of about 65 m, could be distinguished, as shown in Fig. 3.



Fig. 3. Magnetic flux tube visualized by the collisional interaction between an electron beam and Ar background gas.

In contrast to the fluorescent rod measurements, the technique not only results in a Poincaré plot at a fixed toroidal position but also generates a detectable light signal in the whole vacuum vessel. However, only a limited number of toroidal turns of the magnetic field lines are visible. Thus, this method can not replace the flux surface measurements but does provide additional information on the magnetic field structure.

ECR Plasma Heating

The plasma is heated with two 2.45-GHz microwave magnetrons with power of 6 kW and 20 kW. Antennas are installed on the low field side, emitting in ordinary mode (O-mode). Typically, plasmas are generated and heated at $B = 87$ mT or below allowing discharges with a length of 30 min; however, the typical length of a discharge is about 1 min. The electron temperature is about $T_e \approx 10$ eV, and the ion temperature $T_i \approx 2$ eV [6]. Working gases are H_2 , He, and Ar. The plasma density is higher than the cut-off density $n_{\text{cut-off}} = 7.5 \times 10^{16} \text{ m}^{-3}$, due to mode conversion from ordinary O-mode into extraordinary-mode (X-mode) to electrostatic electron Bernstein wave (EBW). The OXB mode conversion process requires launching the high-frequency beam oblique to the magnetic field lines. An optimized O-to-X conversion antenna results in a peaked density profile ~ 12 times higher than the cut-off density and a slightly hollow T_e profile.

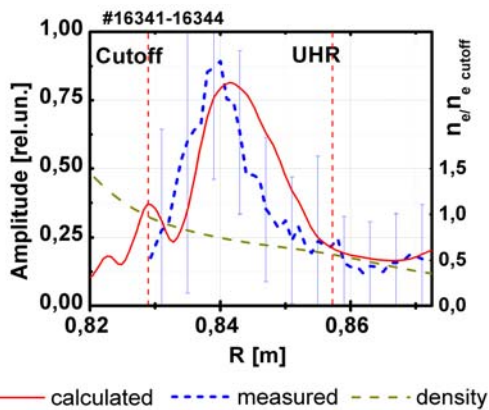


Fig. 4. Radial profiles of measured and FDTD calculated E_y amplitude.

An investigation of plasma heating via OXB mode conversion was performed by measuring the behavior of high-frequency (HF) waves in the WEGA plasma. The set of HF probes was used to measure the amplitude and phase of the heating wave in the vicinity of the heating antenna. Results of the measurements were compared with simulations made using a finite-difference time-domain (FDTD) code. Figure 4 shows that the measurement results agree well with the full-wave calculations. The observed resonant behavior of the wave between the upper hybrid resonant (UHR) layer and cut-off region shows that the conditions for the X-B conversion process are satisfied. The assumption of overdense plasma heating by EBW is

also supported by Langmuir probe measurements of the plasma parameters with simultaneous heating power modulation. The measurements show the deposition of the HF power deep inside the overdense plasma region.

A 20-kW, 28-GHz electron cyclotron resonance heating (ECRH) system has recently been installed on WEGA for plasma production and heating studies at 0.5 T magnetic fields [7]. Initial plasmas were produced with second harmonic extraordinary mode (X2) heating of the plasma with an expanding Gaussian beam launched from an HE_{11} antenna. Initial argon discharges at $|B_0| = 0.5$ T, $\tau = 0.2$, and $p = 1.0 \times 10^{-5}$ mbar produced densities at the R -cutoff of $n_e = 4.9 \times 10^{18} \text{ m}^{-3}$. At slightly lower pressure, $p = 3.0 \times 10^{-6}$ mbar, centrally peaked density and temperature profiles were observed with peak values of $n_e \sim 4 \times 10^{17} \text{ m}^{-3}$, $T_e \sim 5$ eV, $T_i \sim 4$ eV, and a fast electron population of around 200–300 eV.

In the next stage of experiments, a parabolic mirror will be used to focus the Gaussian beam emanating from the end of the waveguide into the center of the plasma where, using ISS95, $\langle T_e \rangle = 50$ eV and $n_e < 5 \times 10^{18} \text{ m}^{-3}$ are expected. The system will be used to generate suprathermal particles for fast-particle confinement studies in different magnetic configurations (various τ) in the stellarator geometry. It can also be used for such studies in stellarator-tokamak hybrids, when a power supply for the WEGA ohmic heating coils is installed. The system will also be used for overdense OXB mode heating of the plasma, using an oblique launch arrangement shown in Fig. 6. Here, using ISS95, $\langle T_e \rangle = 25$ eV and $n_e > 1 \times 10^{19} \text{ m}^{-3}$ are anticipated. This is ideal for wave physics studies and to test W7-X divertor diagnostics.

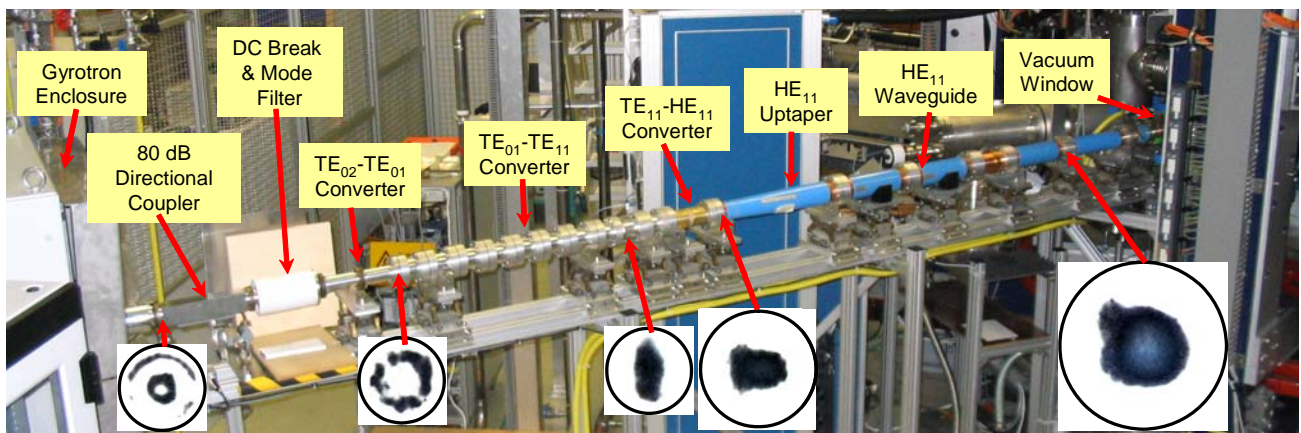


Fig. 5. Configuration of the new 28-GHz ECRH system on WEGA used in initial X2-mode heating experiments. Waveguide mode patterns measured with burn paper are shown below the waveguide, confirming the conversion of the gyrotron TE_{02} output mode into the HE_{11} mode launched into the plasma.

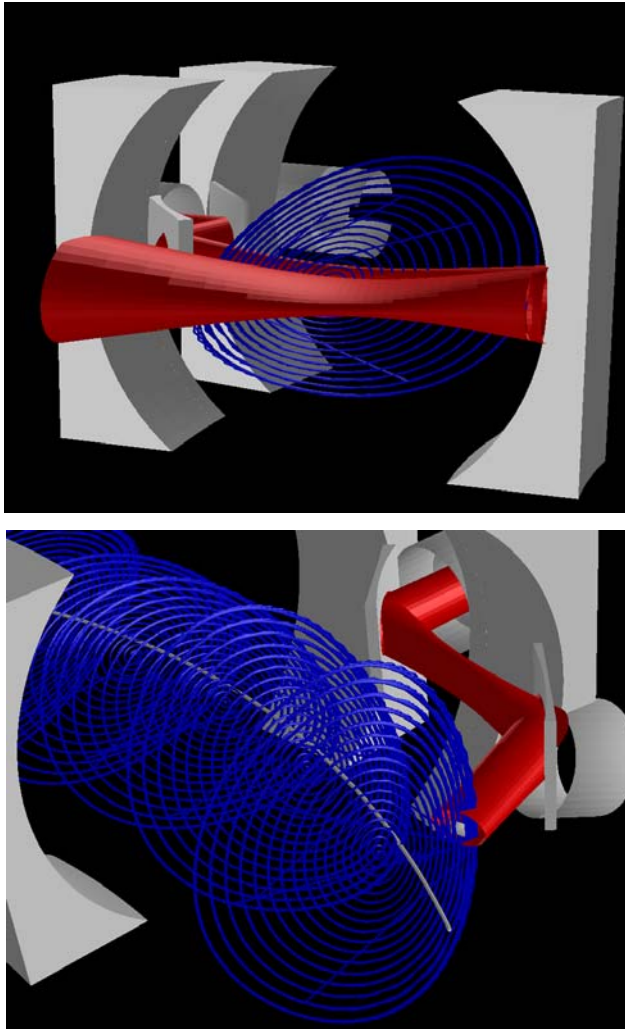


Fig. 6. Launching beam geometry for 28 GHz X2 (top) and OXB (bottom) heating.

Heavy Ion Beam Probe

In collaboration with the Institute for Plasma Physics in Kharkov, Ukraine, a HIBP diagnostic is currently being tested on WEGA [8]. The diagnostic principle is based on the difference of the Larmor radii of highly energetic heavy ions with different ionization states. In WEGA, the primary 40-keV Na^+ beam is injected into a magnetic field of 0.5 T, and a secondary Na^{++} beam is detected as shown in Fig. 7. Energy analysis yields the electrostatic plasma potential inside the secondary ionization volume with an estimated spatial resolution of about 1.5 cm. Radial profile scans are obtained using a deflection system to vary the injection angle. Cross-checks with Langmuir probe data are planned, as well as electric field studies in combination with the 28-GHz gyrotron operation. Because of the strong dependence of the secondary ionization cross section on the electron energy, the secondary signal intensity will be very sensitive to the existence of suprathermal electrons.

The intrinsic temporal resolution is high enough to measure plasma parameters in experiments with modulated heating power. Temporal resolution is limited by the noise level and bandwidth of the amplifiers used in the detection system.

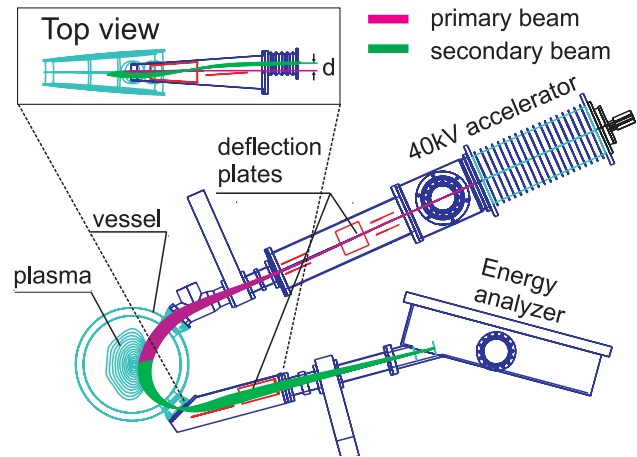


Fig. 7. Schematic of the HIBP system with calculated ion trajectories. Because of the helical magnetic field component, the ions are deflected also in the toroidal direction ($d \approx 3$ cm).

Electrostatic fluctuations

Two probe systems installed at WEGA are designed for poloidally and toroidally resolved studies of electrostatic fluctuations using a poloidal probe array, as shown in Fig. 8 and a single probe separated by 135° in toroidal angle.

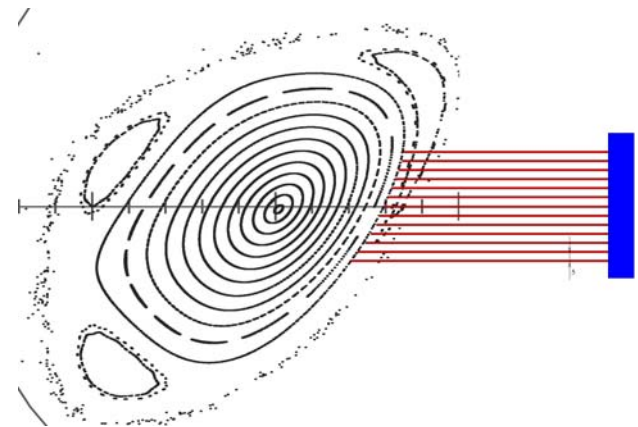


Fig. 8. Poloidal probe array with 13 tips following the flux surface geometry.

Calculations with a field line tracing code show that direct connections parallel to \mathbf{B} exist between the two probe systems for different connection lengths. Their existence has

been verified experimentally for the short connection length. An electron gun has been installed at the single probe position, producing an electron beam parallel to \mathbf{B} . The emitted electron current was detected at a single tip of the probe array, showing the location of the direct connection length.

The spatiotemporal structure of the fluctuations shows the turbulent behavior of the plasma. Figure 9 shows a frequency spectrum of the saturation current I_{sat} fluctuations measured for a standard He discharge at $t = 0.2$ and $B = 57$ mT. This is an example for a configuration with fully developed turbulence. In some magnetic configurations the turbulent spectrum shows additional coherent modes.

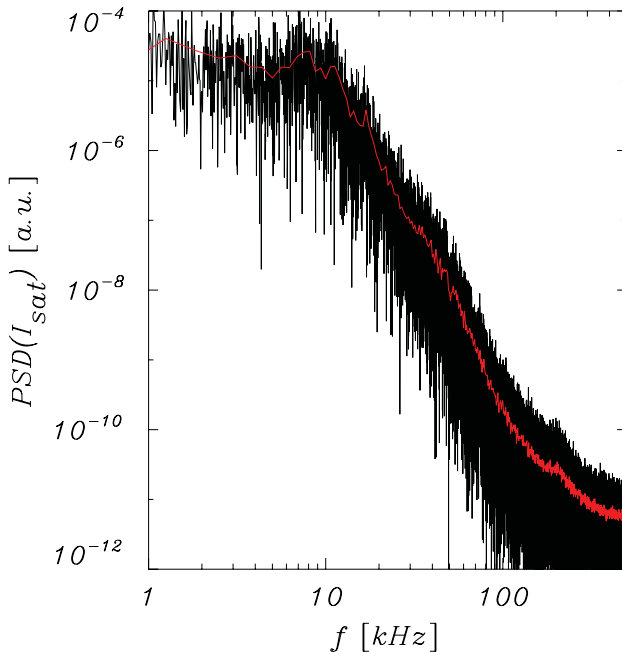


Fig. 9. Power spectrum of I_{sat} fluctuations measured in He. The noise of the original spectrum (black line) is reduced by averaging over neighboring frequencies (red line).

Figure 10 shows a typical radial profile of I_{sat} fluctuations measured in He. The fluctuation amplitude shows a maximum where the density gradient is steepest. The relative fluctuation level of 10–30% was observed in He and H_2 discharges. In Ar, the fluctuation level is much smaller—a few percent. Initial spatially resolved experiments indicate a finite structure size of the fluctuations both perpendicular and parallel to \mathbf{B} . Poloidal correlation lengths are in the range of a few centimeters.

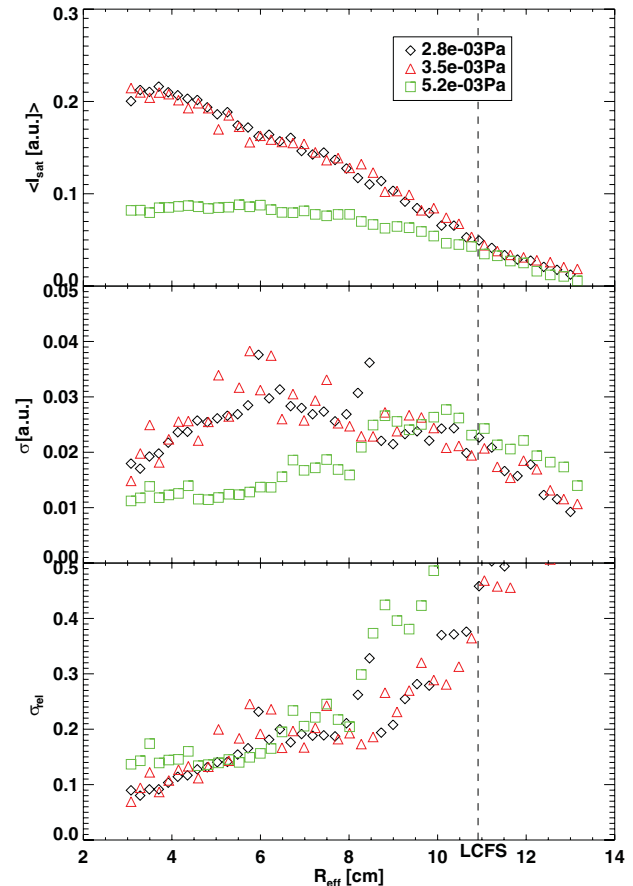


Fig. 10. Radial profiles of I_{sat} measured in He for different pressures. $\langle I_{\text{sat}} \rangle$ is the stationary part of the signal, σ is its standard deviation corresponding to the fluctuation amplitude, and σ_{rel} is the relative fluctuation amplitude.

Experiments on the turbulent transport in the region of magnetic islands are planned. Using a compensation coil it is possible to influence the $m = 1$ islands. This flexibility can be used to place the poloidal probe array in different regions of the island (e.g., at the O- or X-point) and to study turbulence under similar plasma conditions with and without islands.

Coherence Imaging Spectrometer

The spectroscopic systems installed at WEGA currently consist of an ultrahigh-resolution spectrometer and a coherence imaging spectrometer (CIS). Both are used to measure the emissivity of selected lines, ion temperature, and ion flow speed.

A coherent imaging spectrometer is very similar to a Fourier-transform spectrometer. The light coming from the plasma is split into ordinary and extraordinary rays by birefringent crystals. It is then electro-optically modulated. The ordinary and extraordinary rays interfere and the

interferogram is recorded on a camera. The first three moments of the signal correspond to the intensity, ion temperature, and ion speed. The system captures images with a frame rate of ~ 10 Hz, from which plasma flow and temperature are derived. In Fig. 11 the impact parameter is the z -coordinate on the magnetic axis, and ϕ is the intersection of the toroidal angle with the viewing angle on the magnetic axis [9].

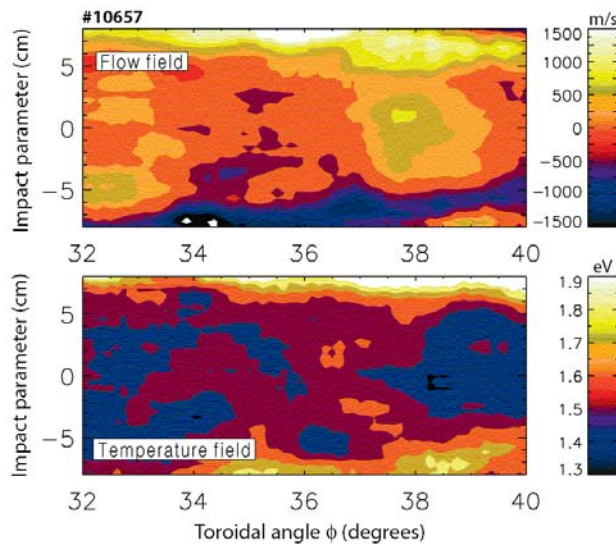


Fig. 11. Plasma flow velocity (above) and ion temperature (below) for He.

Typically Ar ion temperatures are ~ 3 eV, having a maximum near the last closed flux surface. Argon plasmas typically rotate poloidally with a speed of around 1000 m/s near the last closed flux surface. The poloidal rotation of the ions consists of the $\mathbf{E} \times \mathbf{B}$ drift and the ion diamagnetic drift. The drift components are derived from Langmuir probe data. Combining all three systems allows determination of the drift components.

In the future the systems will be used to study the impact of edge biasing on the net ion motion in WEGA. An additional optical emission diagnostic to tomographically derive electron density and temperature from line-ratio measurements is being constructed.

Acknowledgment

The authors are grateful to Michael Laux, Johann Lingertat, Matthias Hirsch, John Howard, Ralf König, Heinrich Laqua, Andreas Werner, Arthur Weller, and Daihong Zhang for their contributions to the experiment and thank Dieter Abmus, Norbert Paschkowski, and Ralf Gerhardt for their technical support.

M. Otte, O. Lischtschenko, S. Marsen, M. Schubert, Y. Y. Podoba, F. Wagner, G. B. Warr
Max-Planck-Institut für Plasmaphysik
Greifswald Branch
17491 Greifswald, Germany
E-mail: matthias.otte@ipp.mpg.de

L.I. Krupnik, A.V. Melnikov, A.I. Zhezhera
NSC KIPT Institute of Plasma Physics
61108, Kharkov, Ukraine
E-mail: HIBP@ipp.kharkov.ua

References

- [1] D. Zhang, M. Otte and L. Giannone, "Bolometer Results in the Long-Microwave-Heated WEGA Stellarator," P-2.03 presented at PLASMA2005 (Int. Conf. on Research and Applications of Plasmas), Poland, 5–9 September 2005.
- [2] M. Otte and J. Lingertat, "Initial Results of Magnetic Surface Mapping in the WEGA Stellarator," Proc. 29th EPS Conf. on Plasma Phys. and Control. Fusion, Montreux, 17–21 June 2002, ECA **26B**, P-5.036 (2002).
- [3] M. Otte, J. Lingertat and F. Wagner, "Operation of the WEGA Stellarator with Vertical Field and Compensation Coils," Proc. 30th EPS Conf. Control. Fusion Plasma Phys., St. Petersburg, 7–11 July 2003, ECA **27A**, P-1.9 (2003).
- [4] G. Gourdon, D. Marty, E. K. Maschke, and J. D. Dumont, Proc. of the Third Int. Conf. on Plasma Phys. Control. Nucl. Fusion Res., Novosibirsk, USSR, 1968 (IAEA, Vienna, 1969) **1**, p. 847.
- [5] A. Werner, Max-Planck-Institut für Plasmaphysik Greifswald, private communication.
- [6] K. Horvath, J. Lingertat, M. Otte, and Friedrich Wagner, Plasma Phys. Control. Fusion **48** (2006) 315–323.
- [7] G. B. Warr, H. P. Laqua, D. Assmus, W. Kasperek, D. Keil, O. Lischtschenko, S. Marsen, M. Otte, M. Schubert and F. Wagner, "New 28 GHz Plasma ECR Heating System for the WEGA Stellarator," presented at the 33rd European Phys. Soc. Conf. on Plasma Phys. Rome, Italy, 19–23 June 2006.
- [8] L. Krupnik et al., "Development of Heavy Ion Beam Probing (HIBP) Diagnostic for Stellarator WEGA," Proc. 15th Int. Stellarator Workshop, P2-11, Madrid (2005).
- [9] J. Chung, R. König, J. Howard, M. Otte and T. Klinger, Plasma Phys. Control. Fusion **47** (2005) 919–940.

Stellarator Workshop database

CIEMAT has undertaken the compilation of a database containing the proceedings of past Stellarator Workshops, since proceedings for many past events are not available via the Internet.

Currently this page is available at

<http://www-fusion.ciemat.es/SW2005/previous.shtml>

and it is currently unfinished. Further information is being added.

Dr. Boudewijn Ph. van Milligen
Asociacion EURATOM-CIEMAT
Avenida Complutense 22, Edif. 66
28040 Madrid, España - Spain
Tel.: (+34)-91-346.6379/6159
E-Mail: boudewijn.vanmilligen@ciemat.es
Web: http://www-fusion.ciemat.es/New_fusion/es/Laboratorio/personal/Boudewijn